Nanoparticle shape selection by repulsive interactions: Metal islands on few-layer graphene

L. A. Somers,[1] N. A. Zimbovskaya,[2,3] A. T. Johnson,[1] and E. J. Mele[1,*]
[1]*Department of Physics and Astronomy, University of Pennsylvania, Philadelphia, Pennsylvania 19104, USA*
[2]*Department of Physics and Electronics, University of Puert Rico–Humacao, CUH Station, Humacao, 00791 Puerto Rico, USA*
[3]*Institute for Functional Nanomaterials, University of Puerto Rico, San Juan, 00931 Puerto Rico, USA*
(Received 22 July 2010; published 17 September 2010)

Metal atoms adsorbed on few-layer graphenes condense to form nanometer-size droplets whose growth is size limited by a competition between the surface tension and repulsive electrostatic interactions from charge transfer between the metal droplet and the graphene. For situations where the work-function mismatch is large and the droplet surface tension is small, a growing droplet can be unstable to a family of shape instabilities. We observe this phenomenon for Yb deposited and annealed on few-layer graphenes and develop a theoretical model to describe it by studying the renormalization of the line tension of a two-dimensional droplet by repulsive interparticle interactions. Our model describes the onset of shape instabilities for nanoparticles where the growth is size limited by a generic repulsive potential and provides a good account of the experimentally observed structures for Yb on graphene.

DOI: 10.1103/PhysRevB.82.115430 PACS number(s): 68.65.Pq, 68.70.+w, 68.37.Lp, 68.43.Hn

I. INTRODUCTION

Graphite is widely used as a substrate for the synthesis of free-standing metal nanoparticles due to its low chemical reactivity, small diffusion barriers for adsorbed species and high degree of structural order. Recent work suggests that graphene can promote the self-assembly adsorbed-metal atoms into nanoscale clusters with controllable size distributions[1,2] potentially opening a new route to nanoparticle synthesis. This mode of nanoparticle growth is attractive since being grown *in situ* the particles can be clean and densely packed without aggregating. The species that are produced may be useful for applications in electronics, optics, information storage, nanofluidics, and catalysis. For example, graphenes grown on Ir(111) often exhibit moiré patterns (resulting from the slight lateral lattice mismatch) which can template the growth of adsorbed-metal species.[1] Microscopic calculations suggest that this occurs due to the differential reactivity of metal species with specific sites of the graphene lattice that are in or out of registry with the Ir support.[3,4] These developments highlight the need for understanding better the mechanisms that control the kinetics and phase behavior of adsorbed species on graphenes.

It is becoming increasingly appreciated that the *thickness* of a few-layer graphene is an important control parameter for the surface energetics and phase behavior of adsorbed species. In our earlier work[2] we observed that when Au atoms are deposited on few-layer graphenes containing m layers where $1 \leq m < 20$, the mode of adatom condensation and nanoparticle growth differs sharply from that observed on thick graphite. On few-layer graphenes Au condenses to form size-limited isotropic droplets as shown in Fig. 1 where the diameter is controlled by the layer count m of the graphene substrate, increasing approximately as $m^{1/3}$. This phenomenon is well described by a model in which electrostatic dipole-dipole repulsion within a condensed-island prevents the continued growth of large droplets. This unusual thickness dependence arises from a short-range cutoff of this repulsive potential which occurs on the scale of the dipole. For few-layer graphenes, which screen poorly when the charge exchange is small, this scale is effectively the thickness of the graphene film.

In this paper we examine the effects of general repulsive interactions on *shape* selection for a condensed two-dimensional system. This work analyzes experiments similar to those of Luo *et al.*[2] where Yb is adsorbed on few-layer graphene films. As shown in Fig. 2 these are observed to condense in filamentary labyrinthine structures rather than in isotropic size-limited droplets, suggesting new physics in the surface energetics. Indeed, Yb is distinguished by a significantly larger work-function mismatch to the graphene and a lower intrinsic surface tension. These two features combine to produce a mode-dependent renormalization of the line tension of a growing isotropic droplet. A shape instability occurs when the line tension for a particular surface mode of

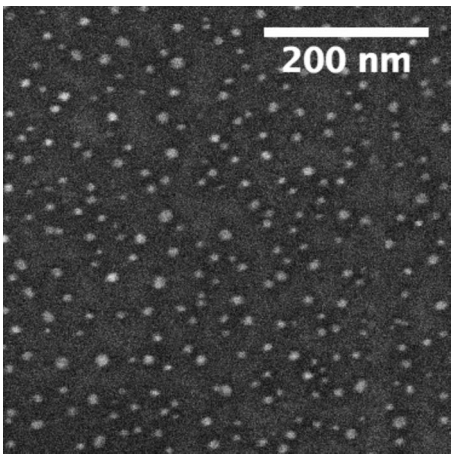

FIG. 1. SEM image of Au islands formed after annealing on four layer graphene. The Au atoms condense to form size-limited nearly isotropic droplets whose radius is limited by the repulsion between perpendicular dipoles at the Au graphene interface. The average droplet radius is determined by the microscopic width of the dipole layer, effectively the width of the few-layer graphene substrate.

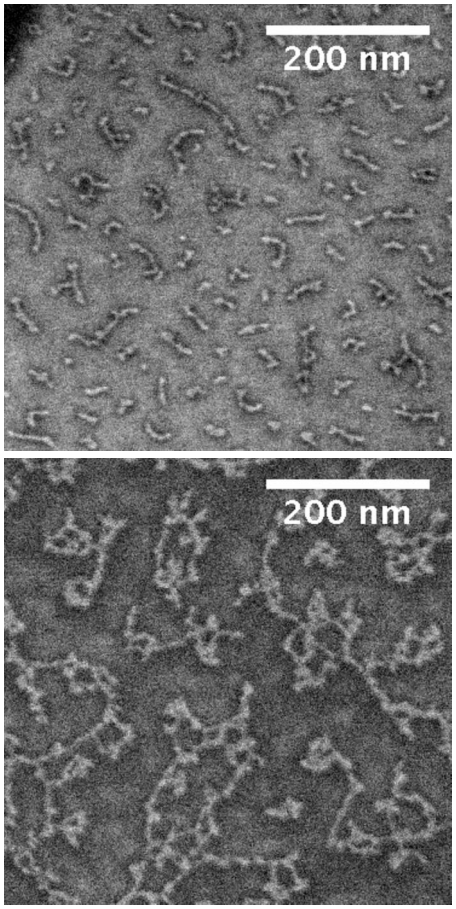

FIG. 2. SEM image of Yb nanoparticles formed after annealing on graphene. The metal atoms condense to form anisotropic fibrillar structures. The top panel is for an average coverage of 0.12 nm and the bottom is for an average coverage of 0.5 nm.

the droplet, constrained to have a constant total area, goes to zero. We develop a formulation describing this shape instability driven by a *general* repulsive potential. For application to Yb/graphene, where this repulsive potential repulsion is provided by electrostatic dipolar interactions and can be calculated from the work-function mismatch, we observe a sign reversal of the mode-dependent surface tension for an isotropic droplet as a function of its radius. This model correctly accounts for the observed widths of the labyrinthine structures and the occasional appearance of threefold and fourfold vertices in the condensed-filamentary patterns. These results provide striking evidence for the essential role of electrostatic interactions in the selection of the shapes as well as sizes of these adsorbed species.

Shape instabilities produced by electrostatic and magnetostatic dipolar interactions often arise in condensed-matter problems. For example, in two dimensions they are associated with the shapes of amphiphile domains at the air water interface[5] (electrostatic) and of ferrofluid droplets[6] (magnetostatic). Langer *et al.*[7] examined this problem theoretically, exploiting the dipolar form of the repulsive interaction. They derived an explicit formula for the line energy of a two-dimensional droplet in terms of a double line integral over its perimeter, a result that, in principle, can be used as input to an algorithm to compute the shape of a growing droplet. This approach was subsequently refined by Iwamoto *et al.*[8,9] who replace the double line integral by an expression for the line energy parameterized by the amplitudes of its modes of deformation, and they applied this method to study effects of dipolar interactions both for the perpendicular geometry and for dipoles tilted with a nonzero component parallel to the tangent plane of the droplet. Our work is similar in spirit to that of Iwamoto *et al.*,[8] though we present it here in a form that is applicable to a general repulsive potential. For the electrostatic dipolar repulsive potential appropriate to the Yb/graphene problem the model provides a good account of the experimental observations. Furthermore this formulation emphasizes that shape instabilities of this type are a generic property of condensed phases of species with repulsive tails in their interaction potentials. Our method can be used to access this physics for a droplet with a general two-point interaction potential in its interior.

Section II of this paper provides more information about our sample preparation, characterization, and imaging of Yb and Au nanoparticles formed on few-layer graphenes. Section III briefly reviews the isotropic model introduced in our earlier paper[2] appropriate to size-limited circular droplets for Au on graphene. Section IV presents some useful formulas for weakly perturbed circular droplets. Section V constructs a model for the droplet energetics including the interaction renormalized line tension. Section VI applied the model to Yb and Au droplets on few-layer graphene and provides comparison of the model with the experimental data. A brief discussion of the results is given in Sec. VII. Some technical details of the calculations are collected in Appendices A and B.

II. EXPERIMENTAL

We prepared graphene flakes by mechanical exfoliation of kish graphite onto 300 nm silicon oxide on silicon wafers. We then cleaned the sample by annealing at 400 C in a reducing atmosphere, 1:1 H_2 and Ar. Individual flakes were identified by color contrast in an optical microscope. Flake thickness was determined by Veeco Dimension 3100 atomic force microscopy in tapping mode.

We then thermally evaporated thin layers of metal onto the surfaces. The deposition thickness was determined by a crystal thickness monitor. We deposited 0.22 ± 0.1 nm and 0.5 ± 0.1 nm of Yb on different chips. For Au samples, the thickness was 0.3 ± 0.1 nm. Each sample was annealed to equilibrium at 600 C (Yb) or 400 C (Au) for three hours in a reducing atmosphere, 1:1 H_2 and Ar.

We then imaged the samples in an FEI DB 235 high-resolution scanning electron microscopy (SEM)/focused ion beam in high-resolution scanning electron microscopy mode. Even short exposures to the beam have been found to contaminate the imaged region and reduce quality so we were especially careful that each image was taken in a previously unimaged area.

Figures 1 and 2 show Au and Yb nanoparticles on single-layer and few-layer graphenes. The Au particles, as noted in [1], are nearly isotropic. The average radius of these nano-

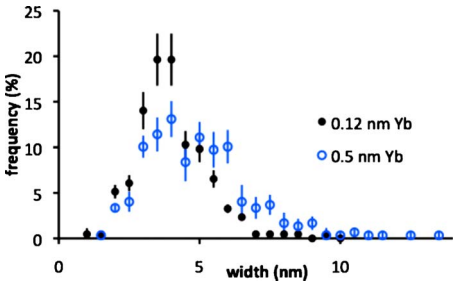

FIG. 3. (Color online) Width distribution of the Yb fibrils displayed in the top and bottom panels of Fig. 2 for the average coverages shown.

particles increases with the thickness of the few-layer graphene substrate. By contrast Yb forms branching strands. The sample with less Yb has strands that are more regular in width. Figure 3 shows histograms of the distribution of Yb strand widths extracted from the images of Fig. 2. The data at higher coverage were obtained over a wider image than shown in the lower panel of Fig. 2. We excluded only places where the Yb was clearly branching. The mean of the distribution for 0.22 nm average coverage is 4.01 ± 0.08 nm, and at a 0.5 nm coverage it increases to is 4.95 ± 0.11 nm. The peaks of the two distributions overlap; the increase arises from the irregularities which are more marked on the sample with more Yb. We also measured the orientations of those Yb strands that have a clear direction. There is no clear deviation from isotropy on the whole.

III. REVIEW OF THE ISOTROPIC MODEL

Our earlier work[2] considers the contribution to the energy of an isotropic droplet, modeled as a short circular cylinder. The energy of a droplet of radius R and height h (Fig. 4) can be expressed

$$U = \gamma(\pi R^2 + 2\pi Rh) + e\pi R^2 h + \Gamma R^4, \tag{1}$$

where γ is the surface tension and e (<0) is bulk cohesive energy density. The last term results from the dipole-dipole interactions and the scaling with R^4 is the essential feature that prevents the growth of large droplets. Note that because of the long-range tail of the electrostatic interaction, the last term can be regarded as a volume-squared contribution to the droplet energy. Evaluation of the coefficient Γ in this expression requires that one regularize the short-range divergence of the $1/r^3$ dipole-dipole potential. Physically this is regularized by the finite spatial extent of the microscopic dipole which we label d. For graphene doped near its charge neutrality point the screening is weak and the distance d may be identified with the thickness of the graphene film.[10] This leads to the central result that the droplet radius is proportional to $d^{1/3}$, which is the scaling rule identified in the experiments studying Au particles on graphene.[2]

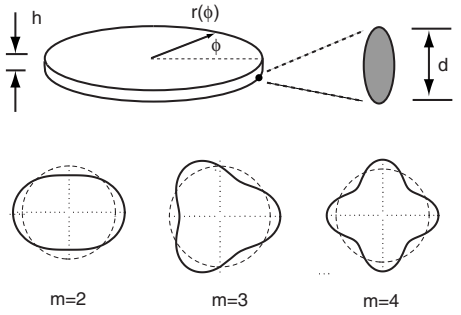

FIG. 4. Diagram illustrating the geometry of the deformed droplet with radius $r(\phi)$, height h, and dipole layer height d. The lower panel illustrates the three modes of deformation with $m=2$, 3, and 4.

The electrostatic contribution in Eq. (1) is obtained by isolating the small momentum $(q \to 0)$ limit of the dipole-dipole interaction.[2] By contrast, the model for the shape instability developed below requires that we extend this into the $q \neq 0$ regime and in fact we show below that the interactions that drive the shape instability are obtained by integrating the interaction over all momenta.

IV. MENSURATION FORMULAS

We are interested in perturbations of a two-dimensional droplet around a reference isotropic (circular) shape. The equilibrium shape is determined by a competition between its volume, surface, and edge energies. Here we parameterize each of these quantities in terms of the deformation amplitudes of a circular droplet.

Referring to Fig. 4, we write the droplet radius as a function of the polar angle

$$r(\phi) = r_0 + \sum_{m \neq 0} r_m e^{im\phi}.$$

Since $r(\phi)$ is real $r_{-m} = r_m^*$. We are considering instabilities around the circular shape and so we consider the situation $r_m \ll r_0$.

The differential length along the tangent line of this curve is

$$d\ell^2 = dr^2 + (rd\phi)^2,$$

which gives a formula for the length of the edge of the droplet

$$\mathcal{L} = 2\pi r_0 + \frac{\pi}{r_0} \sum_m m^2 |r_m|^2.$$

Note that because of the ϕ derivative, the higher m terms are more effective at increasing the arclength and thus tend to be suppressed by a positive surface tension.

The cross-sectional area is given by a line integral over the perimeter

$$\mathcal{A} = \frac{1}{2} \oint \hat{e}_z \cdot (\vec{r} \times d\vec{r}).$$

Since $\vec{r}(\phi) = r(\phi)\hat{e}_r$ one has

$$d\vec{r} = \frac{dr}{d\phi}\hat{e}_r + r(\phi)\hat{e}_\phi,$$

which gives

$$\mathcal{A} = \frac{1}{2}\oint r(\phi)^2 d\phi$$

and integrating over angles gives

$$\mathcal{A} = \pi r_0^2 + \pi \sum_{m\neq 0} |r_m|^2.$$

For a droplet of height h the enclosed volume is simply $\mathcal{V}=\mathcal{A}h$. Any shape change in a droplet that preserves the particle number thus keeps the norm $\mathcal{A}$ constant assuming fixed h. In particular, if we consider an area-preserving deformation characterized by the amplitudes r_m then the isotropic term has to adjust in the manner $r_0'=r_0[r_m] = \sqrt{r_0^2[0]-\Sigma_m|r_m|^2} \approx r_0-(1/2r_0)\Sigma_m|r_m|^2$.

V. DROPLET ENERGY

A. Line energy

The effective droplet line tension arises from the surface energy of the curved sidewalls of the droplet. Thus the tension $\mathcal{T}=\gamma h$ and the line energy is

$$U_{\text{line}} = 2\pi\gamma h\left(r_0' + \frac{1}{2r_0'}\sum_m m^2|r_m|^2\right), \tag{2}$$

where we are truncating the expansion at quadratic order in the r_m. The constant-area constraint can be enforced by rewriting Eq. (2)

$$U_{\text{line}} = 2\pi\gamma h\left[r_0 + \frac{1}{2r_0}\sum_m (m^2-1)|r_m|^2\right]. \tag{3}$$

Note that to quadratic order in the deformations, the $m=1$ term does not change the line energy since it describes a rigid translation of the reference circular droplet.

B. Interaction energy

Two-point interactions within a condensed droplet can modify the effective line tension at its boundary. In this section we develop a formalism for calculating the mode-dependent renormalized line tension working in a constant-area ensemble. One can also derive these results by working in the grand canonical ensemble, allowing for fluctuation in the total droplet area.

We describe the interactions within the droplet by a two-dimensional potential which depends on the lateral separation of two volume elements $V(\vec{r}_1-\vec{r}_2)$. In this problem we are particularly interested in the interactions between parallel electric dipoles mutually oriented along the interface normal with dipole density $\vec{\tau}$. This dipole layer produces a potential step that equilibrates the work-function mismatch between the metal and graphene $\Delta\Phi$ with $\tau=\Delta\Phi/4\pi e$. The electrostatic energy of an island can be expressed as a double integral over the droplet area

$$U_d = \frac{\Delta\Phi^2}{32\pi^2e^2}\int\int d^2r d^2r' f(\vec{r})f(\vec{r}')g(|\vec{r}-\vec{r}'|),$$

where the dimensionless distribution function $f(\vec{r})=1$ inside the droplet and zero outside. It is useful to write this interaction energy as a momentum integral

$$U_d = \frac{\Delta\Phi^2}{32\pi^2e^2}\int \frac{d^2q}{2\pi} v(\vec{q})|S(\vec{q})|^2, \tag{4}$$

where

$$v(\vec{q}) = \int \frac{d^2r}{2\pi} e^{-i\vec{q}\cdot\vec{r}} g(r)$$

and

$$S(\vec{q}) = \int d^2r e^{-i\vec{q}\cdot\vec{r}} f(\vec{r}). \tag{5}$$

At distances large compared to the size of the dipole d, the interaction kernel takes the form

$$\lim_{r\gg d} g(r) \to \frac{1}{r^3},$$

which must be regularized in the near field on the scale of the dipole. A convenient form for the regularized kernel is

$$g(r) = \frac{1}{(r^2+d^2)^{3/2}},$$

which gives

$$v(q) = \frac{1}{d}\exp(-qd) = \frac{1}{d}\tilde{v}(\xi),$$

where $\xi=qd$ defines the dimensionless momentum. Note that the interaction strength scales inversely with the width of the dipole layer d.

The function $S(\vec{q})$ can be parameterized in terms of the coefficients r_m. In Appendix A we show that this can be broken into an isotropic part

$$S_0(q) = \frac{2\pi r_0}{q} J_1(qr_0)$$

and a part that depends on r_m with $m\neq 0$

$$S_m = 2\pi i^m e^{im\phi_q} J_m(qr_0) r_0 r_m.$$

In a similar manner, the interaction energy in Eq. (4) can be partitioned into additive contributions from its isotropic part

$$U_0 = \left(\frac{\Delta\Phi^2}{8e^2d}\right)\int d\xi\tilde{v}(\xi)\frac{J_1^2(\xi r_0/d)}{\xi} r_0^2 \equiv g_0 r_0^2 \tag{6}$$

and its shape-dependent terms given by a sum over m

$$U_{\text{shape}} = \left(\frac{\Delta\Phi^2}{8e^2d}\right)\left(\frac{r_0}{d}\right)^2 \sum_{m\neq 0}\left[\int \xi d\xi\tilde{v}(\xi)J_m^2(\xi r_0/d)\right]|r_m|^2$$
$$\equiv \sum_{m\neq 0} g_m(r_0)|r_m|^2. \tag{7}$$

Note that the coefficient of the $|r_m|^2$ term is always *positive* and thus U_{shape} is positive definite: each mode of deformation makes a positive contribution to the total electrostatic energy. A shape instability arises from a competition between this deformation-induced energy and a compensating change to the isotropic interaction energy which necessarily occurs if

the droplet area (equivalently the number of condensed particles) is held fixed.

C. Area-preserving deformations

The deformation-induced interaction energy and the droplet area both increase $\propto|r_m|^2$ for small deformations. Thus Eq. (7) contains, in addition to the line energy, a part that contributes to the effective area-dependent energy of a droplet. Here we remove this latter piece which simply renormalizes the surface tension (it depends only on the droplet area) and isolate the residual term that contains the pure shape-dependent energy. To do this we write

$$U = U \pm \gamma_{\rm int}\mathcal{A} = \tilde{U} + \gamma_{\rm int}\mathcal{A},$$

where $\mathcal{A}=\pi(r_0^2+\Sigma_m|r_m|^2)$. An appropriate choice of $\gamma_{\rm int}$ removes from the difference energy $\tilde{U}$ its area-dependent part and thus isolates the pure shape-dependent energy. $\tilde{U}$ can be expressed in terms of $\gamma_{\rm int}$ and the coefficients $[g_m]$ of the quadratic terms in the interaction energy defined previously

$$\tilde{U} = (g_0 - \pi\gamma_{\rm int})r_0^2 + \sum_m (g_m - \pi\gamma_{\rm int})|r_m|^2.$$

Setting $\partial\tilde{U}/\partial\mathcal{A}=0$ eliminates the differential area dependence from $\tilde{U}$, solving for $\gamma_{\rm int}$ then gives the contribution of the interaction term to the area-dependent energy

$$\frac{\partial\tilde{U}}{\partial\mathcal{A}} = \frac{1}{2\pi r_0}\frac{\partial\tilde{U}}{\partial r_0} + \sum_m \frac{1}{2\pi r_m}\frac{\partial\tilde{U}}{\partial r_m} - \gamma_{\rm int} = 0.$$

The interaction contribution to the surface tension is therefore

$$\gamma_{\rm int} = \frac{1}{2\pi}\left(\frac{1}{r_0}\frac{\partial}{\partial r_0} + \sum_m \frac{1}{r_m}\frac{\partial}{\partial r_m}\right)\sum_{\text{all n}} g_n|r_n|^2. \tag{8}$$

The residual energy $\tilde{U}=\Sigma_m(g_m-\pi\gamma_{\rm int})|r_m|^2$ contains the shape-dependent energy under the constraint of constant total droplet area.

In the evaluation of $\gamma_{\rm int}$ care must be taken to retain all terms that contribute to the energy $\tilde{U}$ at order $|r_m|^2$, noting that the expansion coefficients $[g_m]$ are themselves function of r_0. In Appendix B we give the results of this calculation which show that the m-dependent terms in $\gamma_{\rm int}\mathcal{A}$ can be organized in ascending powers of the aspect ratio r_0/d. The momentum integrated-coupling strength is *negative* for $m\neq 0$ so that interactions act to destabilize the isotropic shape. In the physically relevant regime in this problem where the droplet radius r_0 is much larger than the width of the dipole layer d, to leading order in the small quantity d/r_0 we find that this interaction contribution simplifies to

$$\tilde{U}_{\rm shape} = -\left(\frac{\Delta\Phi^2}{16e^2r_0}\right)\sum_{m\neq 0}\left(\frac{r_0}{d}\right)^3|r_m|^2. \tag{9}$$

D. Renormalized line tension

Combining our results for the bare line energy Eq. (2) and interaction contribution Eq. (9), for a droplet constrained to have constant area we have

$$\begin{aligned} U_{\rm line} &= \sum_{m\neq 0}\pi m^2\gamma h\frac{|r_m|^2}{r_0} \\ &\quad\times\left\{1-\frac{1}{m^2}\left[1-\Lambda\int d\xi\xi\tilde{v}(\xi)F_m(\xi,z)\right]\right\} \\ &= \sum_{m\neq 0}\pi m^2\gamma h\frac{|r_m|^2}{r_0}\lambda_m, \end{aligned}$$

where $z=r_0/d$ and we define the dimensionless coupling constant

$$\Lambda = \frac{\Delta\Phi^2}{8\pi e^2\gamma h}$$

and the weight function for the mth mode

$$\begin{aligned} F_m(\xi,z) \equiv &-z^3\left[\frac{1+J_0(\xi z)J_2(\xi z)}{2}\right] \\ &-z^4\left[\frac{\xi J_m(\xi z)(J_{m-1}(\xi z)-J_{m+1}(\xi z))}{2}\right]. \end{aligned}$$

Because of the rapid oscillation of the J_m's for large r_0/d the integrated-coupling strength is well approximated by retaining only the *constant* term in its z^3 coefficient; in this approximation the momentum-integrated interaction is independent of m and we have

$$\lambda_m \approx \left\{1-\frac{1}{m^2}\left[1+\frac{\Lambda}{2}\left(\frac{r_0}{d}\right)^3\right]\right\}.$$

Vanishing λ_m signifies the onset of a shape instability in the mth deformation mode. Thus we obtain a simple scaling rule that gives the critical radius at which the mth mode of a circular droplet becomes unstable

$$\frac{r_c(m)}{d} \approx \left[\frac{2(m^2-1)}{\Lambda}\right]^{1/3}. \tag{10}$$

VI. COMPARISON WITH EXPERIMENT

For Yb on graphene we have $\Delta\Phi=2.2$ eV,[11] $\gamma\approx 320$ erg/cm^2,[12] and $h\approx 10^{-7}$ cm which gives $\Lambda\approx .067$. Figure 5 plots the renormalization coefficients λ_m for this coupling strength as a function of r_0/d for $m=2$, 3, and 4. The plot shows that an Yb island grows from an isotropic seed to a radius $r_0/d\sim 4.5$, where the quadrupolar $m=2$ mode becomes unstable. The approximate expression in Eq. (10) gives $r_c(m=2)/d\approx 4.47$ and is indeed very accurate in this regime. Above this critical point one expects an exponential *growth* of the droplet along a single axis, which one can associate with the filamentary structures observed experimentally. The width of such a filament is twice this critical radius; for $d\approx 0.5$ nm we find that filament width is ~ 5 nm in very good correspondence with the average width

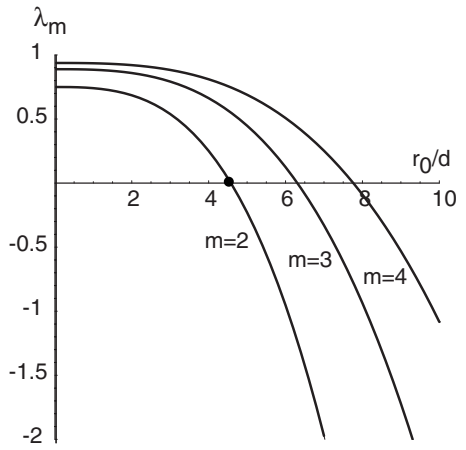

FIG. 5. Line tension renormalization coefficients λ_m plotted as a function of r_0/d for $m=2$, 3, and 4, and for $\Lambda \approx .067$, appropriate to Yb/graphene.

$4.01 \pm .08$ nm computed from the distribution shown in Fig. 3 at 0.12 nm average coverage. As the coverage increases the filaments fold and coarsen due mode competition between the fibrils. The average width in the higher coverage state is thus slightly larger $(4.95 \pm 0.11$ nm). One can contrast this with the situation for Au adsorption on graphene[2] (where $\Delta\Phi \approx 0.5$ eV, $\gamma \approx 1130$ erg/cm^2,[13] and $\Lambda \sim \times 10^{-3}$) which gives $r_c(m=2)/d \approx 20$. This requires growth of a circular droplet to a diameter exceeding 20 nm which is larger than both the intrinsic size limit imposed by the isotropic term in the dipolar energy and the largest droplet sizes observed experimentally for Au on few-layer graphenes.[2]

In general, the stability limits for the isotropic and distorted drops show different scaling with the width of the dipole layer d. A size-limited circular droplet has a radius that increases $\propto d^{1/3}$ while it is stable against shape fluctuations below a critical radius $\propto d$. Thus in the limit of weak coupling (large d) a size-limited circular droplet is stable while for strong electrostatic coupling with $d\sim$ interlayer spacing the droplet can undergo an interaction-driven shape instability. Au and Yb provide examples, respectively, of this weak-coupling and strong-coupling behavior.

VII. DISCUSSION

Three features of Fig. 5 are noteworthy. First, the instability is driven by the terms in our expansion for the shape energy that are quadratic in the deformation amplitudes and have the strongest (highest power) dependence on r_0/d. Thus the instability requires only growth of a droplet past a critical radius for the shape change to occur. At larger r_0/d there is no mechanism that can restore a stable isotropic solution. Thus sufficiently large droplets are absolutely unstable to this type of shape instability. Second, the renormalization coefficient shows that the crossover from the weakly renormalized regime (small r_0) to the unstable regime (large r_0) occurs over a narrow size range. This also reflects the very strong z^3 dependence of the dominant term in the integrated coupling strength. Thus one expects the fibrils to show a sharply peaked width distribution, as is demonstrated experimentally

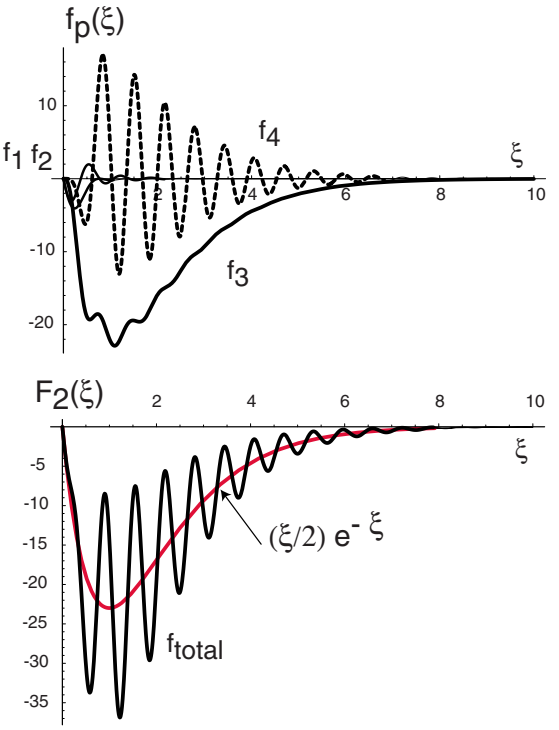

FIG. 6. (Color online) Momentum dependence of the integrand for evaluation of shape-dependent interaction energy for $m=2$ plotted as a function of the dimensionless momentum $\xi=qd$, broken into separate contributions f_p sorted by their dependence on $(r_0/d)^p$ (top panel) and the total (bottom panel). The thin (red) line in the bottom panel plots an expression discussed in the text that provides a good approximation to the integrated coupling strength. The data are presented for $r_0/d=5$.

in Fig. 3. Third, it is striking that the integrated-coupling strength is nearly the same for all the modes of deformation of the circular droplet. Ultimately the shape instability is suppressed for large m modes because of the m^2 scaling of the *bare* line tension rather than through the residual m dependence in the interaction contribution. This leads to our simple scaling rule for the m-dependent critical radii.

Finally, we note that previous continuum formulations of this problem inevitably require a finite droplet height to regularize the short-distance singularity in the dipole-dipole potential when they are treated as *point* dipoles.[7,8] In our treatment this is regularized more naturally by representing the interaction potential using a nonsingular near field form controlled by the finite size of the relevant *microscopic* dipoles. More generally our expression for the interaction-renormalized line energy now can be applied to any repulsive two-point potential in the droplet interior. Indeed, the scaling form for F_m describes the renormalization of the line tension by any nonsingular bulk interaction.

ACKNOWLEDGMENTS

This work was supported by the Department of Energy under Grant No. DE-FG02-ER45118 (E.J.M.), by the National Science Foundation under PREM Grant No. 0353730 (N.A.Z.) and by the NSF under Grant No. DMR08-05136

(L.S. and A.T.J.). We thank Z. Luo and P. Nelson for helpful discussions.

APPENDIX A: FORM FACTORS FOR DEFORMED CIRCULAR DROPLETS

In this appendix we parameterize the form factor of Eq. (5) in terms of the shape coefficients r_m. Consider the Fourier integral over the area of the droplet

$$S(\vec{q}) = \int d\phi r dr e^{-i\vec{q}\cdot\vec{r}} f(\vec{r})$$

$$= \int_0^{r_0} e^{-i\vec{q}\cdot\vec{r}} r dr d\phi + \int_{r_0}^{r_0+\Sigma_m r_m e^{im\phi}} e^{-i\vec{q}\cdot\vec{r}} r dr d\phi.$$

Here the isotropic part gives

$$S_0(q) = 2\pi \int_0^{r_0} J_0(qr) r dr = \frac{2\pi r_0}{q} J_1(qr_0)$$

while the anisotropic piece can be decomposed by noting that $r_m \ll r_0$ and thus

$$S_m = 2\pi i^m e^{im\phi_q} J_m(qr_0) r_0 r_m$$

and therefore we have that

$$S(\vec{q}) = \frac{2\pi r_0}{q} J_1(qr_0) + 2\pi \sum_m i^m e^{im\phi_q} J_m(qr_0) r_0 r_m.$$

These expressions are inserted into the momentum integral for the interaction energy and the angular integration then gives the results in Eqs. (6) and (7).

APPENDIX B: INTERACTION CONTRIBUTION TO THE SURFACE TENSION

The interaction contribution to the surface tension $\gamma_{\rm int}$ is obtained by carrying out the derivatives in Eq. (8) on the quadratic expression for the interaction energy. In this calculation we retain all terms that contribute to the energy $\tilde{U}$ at order $|r_m|^2$, noting that the expansion coefficients $[g_m]$ are themselves function of r_0. The m-dependent terms in $\gamma_{\rm int}\mathcal{A}$ can then be organized in ascending powers of the aspect ratio r_0/d

$$\gamma_{\rm int}\mathcal{A} = \left(\frac{\Delta\Phi^2}{8e^2 r_0}\right) \sum_{m\neq 0} |r_m|^2 \int d\xi \xi \tilde{v}(\xi)$$

$$\times \left(\frac{r_0}{d}\right) \frac{J_1^2(\xi r_0/d)}{\xi^2}$$

$$+ \left(\frac{r_0}{d}\right)^2 J_1(\xi r_0/d) \left[\frac{J_0(\xi r_0/d) - J_2(\xi r_0/d)}{2\xi}\right]$$

$$+ \left(\frac{r_0}{d}\right)^3 \left[J_m^2(\xi r_0/d) + \frac{1 - J_0^2(\xi r_0/d)}{2}\right]$$

$$+ \left(\frac{r_0}{d}\right)^4 \xi J_m(\xi r_0/d) \left[\frac{J_{m-1}(\xi r_0/d) - J_{m+1}(\xi r_0/d)}{2}\right].$$

When r_0/d is large, this expression is controlled by its terms that increase most rapidly as a function of r_0/d. We observe that the first term at $\mathcal{O}(r_0/d)^3$ exactly cancels the "bare" contribution of the mth mode to the interaction energy. The remaining term at $\mathcal{O}(r_0/d)^3$ ultimately dominates the momentum integral since the last term is a rapidly oscillating function of ξ as illustrated in Fig. 6. The momentum-integrated interaction is seen to be *negative* indicating that for area-preserving deformations repulsive interparticle interactions destabilize the isotropic shape at sufficiently large radius. To leading order in the small quantity d/r_0 this is well approximated by the expression in Eq. (9). The lower panel of Fig. 6 compares the full momentum dependent integrand for the interaction strength to an approximate form that retains only the constant coefficient in the z^3 term.

*mele@physics.upenn.edu

[1] A. T. N'Diaye, T. Gerber, C. Busse, J. Mysliveček, J. Coraux, and T. Michely, New J. Phys. **11**, 103045 (2009).

[2] Z. Luo, L. A. Somers, Y. Dan, T. Ly, N. J. Kybert, E. J. Mele, and A. T. Charlie Johnson, Nano Lett. **10**, 777 (2010).

[3] A. T. N'Diaye, S. Bleikamp, P. J. Feibelman, and T. Michely, Phys. Rev. Lett. **97**, 215501 (2006).

[4] P. J. Feibelman, Phys. Rev. B **77**, 165419 (2008).

[5] P. A. Rice and H. M. McConnell, Proc. Natl. Acad. Sci. U.S.A. **86**, 6445 (1989).

[6] M. Seul, L. R. Monar, L. O'Gorman, and R. Wolfe, Science **254**, 1616 (1991).

[7] S. A. Langer, R. E. Goldstein, and D. P. Jackson, Phys. Rev. A **46**, 4894 (1992).

[8] M. Iwamoto and Z.-c. Ou-Yang, Phys. Rev. Lett. **93**, 206101 (2004).

[9] M. Iwamoto, F. Liu, and Z.-c. Ou-Yang, J. Chem. Phys. **125**, 224701 (2006).

[10] An explicit formula for the d-independent coefficient in terms of the work-function mismatch is presented in Luo *et al.* (Ref. 2).

[11] M. V. Nikoli, S. M. Radi, V. Mini, and M. M. Risti, Microelectron. J. **27**, 93 (1996).

[12] *CRC Handbook of Chemistry and Physics*, 82nd ed. (CRC, Boca Raton, 2001).

[13] W. R. Tyson and W. A. Miller, Surf. Sci. **62**, 267 (1977).